



OPEN ACCESS

EDITED BY Alex J. Poulton, Heriot-Watt University, United Kingdom

REVIEWED BY
Zunli Lu,
Syracuse University, United States
George W. Luther,
University of Delaware, United States

*CORRESPONDENCE Yun-Ju Sun ⊠yj.sun@bristol.ac.uk

RECEIVED 20 July 2023 ACCEPTED 18 October 2023 PUBLISHED 07 November 2023

CITATION

Sun Y-J, Robinson LF, Parkinson IJ, Stewart JA, Lu W, Hardisty DS, Liu Q, Kershaw J, LaVigne M and Horner TJ (2023) Iodine-to-calcium ratios in deepses scleractinian and bamboo corals. Front. Mar. Sci. 10:1264380. doi: 10.3389/fmars.2023.1264380

COPYRIGHT

© 2023 Sun, Robinson, Parkinson, Stewart, Lu, Hardisty, Liu, Kershaw, LaVigne and Horner. This is an open-access article distributed under the terms of the Creative Commons Attribution License (CC BY). The use, distribution or reproduction in other forums is permitted, provided the original author(s) and the copyright owner(s) are credited and that the original publication in this journal is cited, in accordance with accepted academic practice. No use, distribution or reproduction is permitted which does not comply with these terms.

Iodine-to-calcium ratios in deep-sea scleractinian and bamboo corals

Yun-Ju Sun^{1*}, Laura F. Robinson^{1,2}, Ian J. Parkinson¹, Joseph A. Stewart¹, Wanyi Lu³, Dalton S. Hardisty⁴, Qian Liu¹, James Kershaw¹, Michèle LaVigne⁵ and Tristan J. Horner⁶

¹School of Earth Sciences, University of Bristol, Bristol, United Kingdom, ²Department of Environment and Geography, University of York, York, United Kingdom, ³Department of Geology and Geophysics, Woods Hole Oceanographic Institution, Woods Hole, MA, United States, ⁴Department of Earth and Environmental Sciences, Michigan State University, East Lansing, MI, United States, ⁵Department of Earth and Oceanographic Science, Bowdoin College, Brunswick, ME, United States, ⁶Department of Marine Chemistry and Geochemistry, Woods Hole Oceanographic Institution, Woods Hole, MA, United States

The distribution of dissolved iodine in seawater is sensitive to multiple biogeochemical cycles, including those of nitrogen and oxygen. The iodineto-calcium ratio (I/Ca) of marine carbonates, such as bulk carbonate or foraminifera, has emerged as a potential proxy for changes in past seawater oxygenation. However, the utility of the I/Ca proxy in deep-sea corals, natural archives of seawater chemistry with wide spatial coverage and radiometric dating potential, remains unexplored. Here, we present the first I/Ca data obtained from modern deep-sea corals, specifically scleractinian and bamboo corals, collected from the Atlantic, Eastern Pacific, and Southern Oceans, encompassing a wide range of seawater oxygen concentrations (10-280 μmol/kg). In contrast to thermodynamic predictions, we observe higher I/Ca ratios in aragonitic corals (scleractinian) compared to calcitic corals (bamboo). This observation suggests a strong biological control during iodate incorporation into deep-sea coral skeletons. For the majority of scleractinian corals, I/Ca exhibits a covariation with local seawater iodate concentrations, which is closely related to seawater oxygen content. Scleractinian corals also exhibit notably lower I/Ca below a seawater oxygen threshold of approximately 160 µmol/kg. In contrast, no significant differences in I/Ca are found among bamboo corals across the range of oxygen concentrations encountered (15-240 μmol/kg). In the North Atlantic, several hydrographic factors, such as temperature and/or salinity, may additionally affect coral I/Ca. Our results highlight the potential of I/Ca ratios in deep-sea scleractinian corals to serve as an indicator of past seawater iodate concentrations, providing valuable insights into historical seawater oxygen levels.

KEYWORDS

biogenic carbonate, iodate incorporation, seawater oxygenation proxy, dissolved oxygen, marine redox state

1 Introduction

Iodine, a biophilic element, circulates between the hydrosphere, atmosphere, and biosphere and plays important roles in Earth's biogeochemical cycles (Carpenter et al., 2021). For example, the ocean is the dominant source of iodine to the atmosphere and the predominant sink for the tropospheric ozone (Carpenter et al., 2013). Because iodine is a redox-sensitive element, its speciation and distribution in the ocean has been linked to primary productivity (Farrenkopf and Luther, 2002), benthic processes (Cutter et al., 2018; Moriyasu et al., 2020), and ocean oxygenation (Lu et al., 2020c). Therefore, understanding the behavior of marine iodine provides insights into both biogeochemical processes and ocean circulation.

In the ocean, iodine has two stable inorganic species, iodate (IO3, the oxidized form) and iodide (I, the reduced form). The reduction of the iodate to iodide is related to dissolved oxygen content and has a similar redox potential and Gibbs free energy to that of the nitrate-nitrite redox couple (Figure 1; Farrenkopf et al., 1997; Rue et al., 1997; Luther, 2023). The concentration of total inorganic iodine in the ocean is generally conservative (450 to 500 nM; Chance et al., 2014) with a long residence time (~300 thousand years; Broecker and Peng, 1982). Seawater iodine speciation is primarily controlled by two processes: in situ redox reactions (Rue et al., 1997) and regional water-mass mixing (Evans et al., 2020; Hardisty et al., 2021). In situ transformation refers to the processes of iodate reduction to iodide in anoxic conditions and iodide re-oxidation to iodate in oxic waters. Under oxic conditions, iodate is the dominant species in the water column (Truesdale et al., 2000). Elevated iodide and low iodate are observed in low oxygen

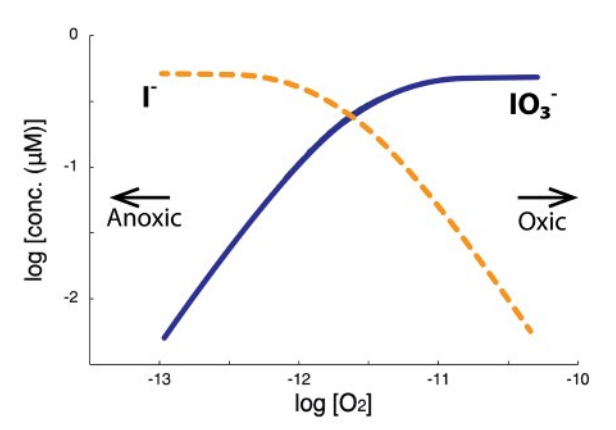


FIGURE 1 Iodine speciation against oxygen concentration constrained by the reaction $IO_3^- \leftrightarrow I^- + \frac{3}{2}O_{2 \text{ (aq)}}$ with standard hydrogen electrode potential $E^0 = -0.144 \text{V}$ at 1 atm and 298 K (Haynes, 2014) with Henry's law constant = 1.3×10⁻³ (mole/L/atm). This calculation assumes ideal solution behaviour and a total iodine concentration of 0.5 μM. The equilibrium constant (K) of the above reaction can be equated with concentration through $K = \frac{|\Gamma|[O_1]^{3/2}}{|O_3|} = e^{\frac{-4G}{84}}$, where [/], $[IO_3^-]$, and $[O_2]$ represents the dissolved concentration of iodide, iodate, and oxygen, respectively. ΔG is the Gibbs free energy of the above reaction and is equated with the standard electrode potential via $\Delta G = -zFE^0$, where z is the number of electrons transferred (z = 6 in this case) and F is the Faraday constant.

regions, such as oxygen minimum zones (OMZs) and deep anoxic basins (Wong and Brewer, 1977; Cutter et al., 2018; Rapp et al., 2020). The asymmetric reaction rates of iodide oxidation and iodate reduction complicate the relationship between iodine and oxygen, decoupling the relative concentrations in the subsurface ocean (Hardisty et al., 2021). In addition, mixing of water masses with different iodate concentrations from adjacent regions influences the seawater iodate concentration. For example, relatively slow reduction rates and elevated offshore Γ concentrations are found in areas like the Eastern Tropical North Pacific (Hardisty et al., 2021), and excess Γ concentrations can also come from sedimentary inputs (Farrenkopf and Luther, 2002; Cutter et al., 2018; Moriyasu et al., 2020; Moriyasu et al., 2023).

Building on field observations, the iodine-to-calcium ratio (I/ Ca) in marine carbonates can potentially record the redox state in seawater, with higher carbonate I/Ca assumed to record higher IO3and therefore higher oxygen concentrations in seawater. This potential is based on the premise that iodate is the only species of iodine incorporated into carbonate (Lu et al., 2010); indeed, computational simulations have confirmed that iodate substitutes for the carbonate ion in the lattice (Podder et al., 2017; Kerisit et al., 2018). The theory that iodate is the sole species of iodine incorporated into carbonates has also been demonstrated experimentally for calcite (Zhou et al., 2014) and dolomite (Hashim et al., 2022). Hence, both marine carbonates have been applied to study oxygenation across different timescales throughout Earth's history (Lu et al., 2020c). Moreover, as iodate reduction does not occur before the dissolved oxygen is depleted to a threshold of ~11 µmol/kg (Hardisty et al., 2021), the I/Ca proxy can serve as a semi-quantitative proxy that puts qualitative constraints on oxygen concentration. Based on globally distributed core-top planktic foraminiferal samples, a threshold I/Ca value (~2.5 µmol/mol) was proposed to indicate hypoxic O2 conditions (~70 to 100 µmol/kg) in the upper water column (Lu et al., 2020b; Lu et al., 2016). Furthermore, data from benthic (epifaunal) foraminifera suggested that low benthic I/Ca value (<3 µmol/mol) indicated low bottom water oxygen (<50 µmol/kg) (Lu et al., 2020b). However, applying foraminiferal I/Ca as an oxygenation proxy has its limitations: planktic foraminifera migrate vertically during their living cycles thus complicating the reconstruction of in situ oxygen level (Lu et al., 2020a), the change of benthic microhabitat (e.g., migration to deeper sediments where a sharp oxygen gradient within the pore water occurs), and subsequent diagenetic processes (e.g., aragonite recrystallisation) could potentially influence benthic foraminiferal I/Ca values (Glock et al., 2014).

Deep-sea corals (DSCs) are valuable palaeoceanographic archives of intermediate- and deep-ocean conditions. They can be accurately and precisely dated by radiometric methods (Cheng et al., 2000), which allows for studying the leads and lags of the climate system on millennial timescales (e.g., Chen et al., 2023). Moreover, DSCs thrive across a wide geographic and bathymetric distribution range (Roberts et al., 2006) and have even been found within the hypoxic zone in Southeast Atlantic (Hebbeln et al., 2020; Orejas et al., 2021) and Northeast Pacific (Ross et al., 2020). Numerous elemental and isotopic ratios have already been developed as environmental proxies in DSCs (e.g., Li/Mg ratio,

radiocarbon, neodymium isotopes; Robinson et al., 2014) and thus DSCs are an appealing archive of iodine geochemistry. Despite this potential, there have been no systematic investigations of I/Ca in DSCs. In this study, we investigate iodine geochemistry in two modern DSC taxa: Scleractinia (aragonite-structured) and bamboo corals (calcite-structured) from across the global ocean (Atlantic Ocean, Eastern Pacific, and Southern Ocean). We examine the mechanisms of iodate incorporation into DSCs, explore the relationship between I/Ca in DSCs and ambient seawater properties, and assess the potential of I/Ca in DSCs as an oxygenation proxy.

2 Samples and methods

2.1 Deep-sea coral sample collection

We analyzed deep-sea scleractinian coral skeletons (n=63) and bamboo coral skeletons (n=13) collected from the Labrador Sea (RRS Discovery DY081), the Rockall Bank in the Northeast Atlantic (RRS James Cook JC136), the tropical North Atlantic (RRS James Cook JC094), the southwest Atlantic (collection from National Historical Museum, Brazil), the Drake Passage region of the Southern Ocean (R/ V Nathaniel B. Palmer 1103), the northeast Pacific (R/V Western Flyer in the year 2004 and 2007), the Marquesas Islands in the central equatorial Pacific (R/V Alis MUSORSTOM 9; collection from National Museum of Natural History, France), and the Galápagos Archipelago (R/V Melville MV1007; Alucia AL1508; E/V Nautilus NA064) (Figure 2). Sample depths ranged from 60 to 2800 m. The majority of deep-sea corals in this study were collected alive with organic tissue attached using a Remotely Operated Vehicle (ROV). If live samples were not available, selected sub-fossil specimens preserved in pristine condition with radiometric ages < 50 years were used (Galápagos samples, n=3; Northeast Atlantic samples, n=4; Equatorial Atlantic samples, n=6), which can be treated as "modern" corals (dating method taken from Chen et al., 2015). The ages of the

California margin's bamboo corals are adapted from radiocarbon analyses (Frenkel et al., 2017). All the corals were paired with available hydrographic data from seawater observational data (see below). Coral samples in this study are subgrouped by location, and the dominant water masses are listed in Table 1.

We grouped DSC by taxonomic order and their distinct mineralogy for further comparison. First, scleractinian coral samples include solitary genera *Balanophyllia*, *Caryophyllia*, *Desmophyllum*, and the colonial genus *Enallopsammia*. The skeletal mineralogy of these scleractinian corals is aragonite. Second, bamboo corals belong to the *Isidella* and *Keratoisis* subfamilies with high-Mg calcitic mineralogy. The full coral sample metadata are included in Supplementary Table 1.

2.2 Hydrographic data

Concentrations of seawater iodate and iodide data were taken from published sources (Wong and Brewer, 1977; Elderfield and Truesdale, 1980; Bluhm et al., 2011; Cutter et al., 2018; Moriyasu et al., 2020; Rapp et al., 2020). Station sites were selected in the closest proximity to the coral site, and the representative value was interpolated from the two closest available measurement depths. Measured seawater iodate/iodide data for the modern ocean, especially depth profiles, remain limited. As a result, some locations and deeper depths lack paired seawater values (e.g., Vayda Seamount in the Equatorial Atlantic). The time-series seawater iodine records have supported the use of single-point sources of seawater data (Campos et al., 1996). The largest published analytical precision for seawater data was 1% (RSD) (Rue et al., 1997). The uncertainty for each seawater iodate/iodide value was estimated from vertical variation between the three most proximal measurements at each coral location (± 2 SD).

The paired dissolved oxygen and hydrographic data (temperature, salinity, [CO₃²⁻], pH, concentrations of nitrate, phosphate, and silicate) for coral samples were taken from

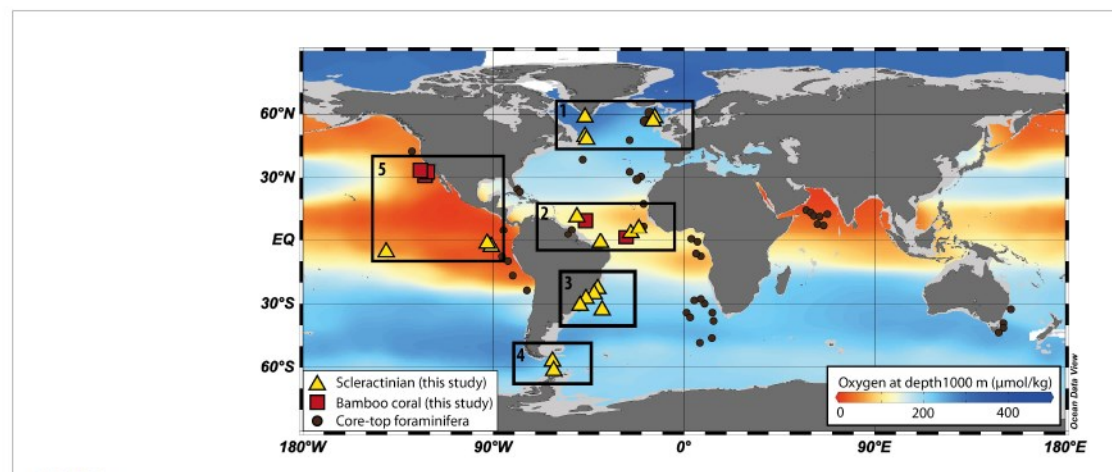


FIGURE 2

Base map illustrating the global mean distribution of oxygen concentrations from GLODAP2 database at 1000 m water depth (Lauvset et al., 2022). The deep-sea coral sample locations are marked as triangles (scleractinian corals) and squares (bamboo corals), including the North Atlantic (location 1), Tropical North Atlantic (location 2), Southwest Atlantic (location 3), Southern Ocean (Atlantic sector; location 4), Eastern Pacific (location 5). The locations of benthic foraminifera data (black dots) are from published studies (Glock et al., 2014; Lu et al., 2020b; Lu et al., 2022).

TABLE 1 Location and depth range of deep-sea coral samples in this study, along with the dominant water mass.

Location	Site	Latitude, Longitude	Coral depth range	Dominant water mass
North Atlantic	Labrador Sea	50.1°N, 45.4°W	1055-2700 m	Labrador Sea Water (LSW) ^a
	North Rockall Bank	58.9°N, 13.4°W	580-1165 m	subpolar Mode Water (SPMW) ^a
Tropical North Atlantic	Carter Seamount	9.2°N, 21.3°W	300-1080 m	Antarctic Intermediate Water (AAIW) ^b
			1260-2400 m	North Atlantic Deep Water (NADW) ^b
	Knipovich Seamount	5.6°N, 26.9°W	300-1080 m	Antarctic Intermediate Water (AAIW) ^b
			1260-2400 m	North Atlantic Deep Water (NADW) ^b
	Vayda Seamount	14.9°N, 48.2°W	1455 m	North Atlantic Deep Water (NADW) ^b
Southwest Atlantic	Rio Grande Rise	30.2°S, 36.9°W	240-950 m	Antarctic Intermediate Water (AAIW) ^c
			1050-1510 m	upper Circumpolar Deep Water (uCDW)c
	Brazilian continental margin	20.5-27.0°S, 38.0-47.0°W	240-950 m	Antarctic Intermediate Water (AAIW) ^c
			1050-1510 m	upper Circumpolar Deep Water (uCDW)c
	West Equatorial Atlantic	2.3°S, 38.3°W	240-950 m	Antarctic Intermediate Water (AAIW) ^c
			1050-1510 m	upper Circumpolar Deep Water (uCDW)c
Southern Ocean (Atlantic sector)	Drake Passage	54.5°S, 62.2°W	315 m	Subantarctic Mode Waters (SAMW) ^d
			1400-1900 m	Antarctic Intermediate Water (AAIW) ^d
Eastern Pacific	California Margin	33.2-37.4°N, 120.9-123.4°W	870-1500 m	Antarctic Intermediate Water (AAIW) ^e
			2055 m	Pacific Deep Water (PDW) ^e
	Marquesas Islands (Central Pacific)	7.9°S, 140.7°W	160-285 m	South Pacific Central Water (SPCW) ^e
	Galápagos Archipelago	0.4-1.2°N, 90.6-91.3°W	250-300 m	13°C water mass (13CW) ^f
			450-500 m	Antarctic Intermediate Water (AAIW) ^f

The map view is shown in Figure 2. References from García-Ibáñez et al. (2018)^a, Liu and Tanhua (2021)^b, Sumida et al. (2020)^c, Hartin et al. (2011)^d, Peters et al. (2018)^c, Evans et al. (2020)^f. The hydrographic properties of paired water masses are listed in Supplementary Table 2.

sensor-mounted CTD/ROV measurements or extracted from the GLODAP2 bottle database (Lauvset et al., 2022). The uncertainty on dissolved oxygen estimates is based on the three most proximal measurements. The oxygen content of the Galápagos site is from the nearest published site (Salinas-de-León et al., 2020). These measurements were all within 300 km and 100 m water depth of coral sampling sites. The seawater [CO₃²⁻] was obtained using the CO2sys.xls program (Pelletier et al., 2007). The input parameters were alkalinity and dissolved inorganic carbon from the GLODAP2 bottle database with dissociation constants taken from Dickson and Millero (1987). All paired seawater data are reported in Supplementary Table 1.

2.3 Sample preparation

Coral samples were treated in bleaching solution (30% v/v sodium hypochlorite solution (reagent grade, Fisher Scientific) in water; ~5% active Cl) after collection and air-dried before physical scraping to remove attached organic matter. A diamond-coated

rotary blade was used to cut pieces of each coral for analysis. We applied coral sampling criteria as described by Stewart et al. (2020): Only coral theca walls were sampled to avoid microstructural bias, such as from highly contrasting trace metal chemistry in centers of calcification (Gagnon et al., 2007). Coral fragments (~1 g) were then finely crushed using a pestle and mortar to provide a homogeneous powder. Most coral samples were prepared at the University of Bristol, and the bamboo coral samples from the California margin were prepared at the University of California, Davis.

The I/Ca coral sample preparations were modified from Lu et al. (2022). Approximately 5 mg of the coral powder was taken for each sample. The cleaning procedure only involved MQ water cleaning for potential day contamination. This cleaning step is critical in I/Ca measurements of foraminifera (Winkelbauer et al., 2021) and we included it for completeness; however, we note for coral samples clay contamination is generally negligible. Neither oxidative nor reductive cleaning steps were applied to best preserve volatile iodine from loss during sample preparation. Reductive cleaning was considered unnecessary as Fe-Mn coatings contain a limited iodine (Zhou et al., 2014). Organic matter in DSCs was removed

in previous steps via physical scraping and treatment in dilute sodium hypochlorite solution.

For most samples, Mg/Ca measurements were conducted alongside iodine measurements. However, for those samples that required separate analysis due to the use of a different instrument (see below), trace element analysis (e.g., Mg/Ca, Mn/Ca) was performed using separate sample aliquots. Those samples were prepared following methods by Barker et al. (2003) and Stewart et al. (2020). Briefly, samples (~5 mg) underwent reductive cleaning (warm bath in 80°C, 3.5% hydrous hydrazine buffered in citric acid/ammonia), oxidative cleaning (warm bath in 80°C, 1% H₂O₂ buffered in ammonia), and weak acid polish (0.0005 M HNO₃). The samples were then dissolved in 0.5 M HNO₃, with a final diluted aliquot containing 4 mM [Ca] taken for analysis. The Mg/Ca of the California Margin bamboo corals were taken from Geyman et al. (2019).

2.4 Analytical techniques

To prepare the samples for iodine measurement, cleaned coral samples were dissolved in 3% HNO3 buffered by 2% tetramethylammonium hydroxide (TMAH) to stabilize the iodine. Dissolved samples were then stored at 4°C. Iodine concentrations were measured the next day in diluted solutions containing ~50 ppm Ca, 5 ppb internal standards (Sc, In, Cs), 0.5% TMAH, and 0.5% nitric acid. The pH of the solution was controlled (pH = \sim 2) to minimize iodine volatilization (Cook et al., 2022). DSC I/Ca analyses were carried out on a Thermo Scientific iCAP Q reverse quadrupole inductively coupled plasma mass spectrometer (ICP-MS) at Woods Hole Oceanographic Institution and a Thermo Scientific iCAP triple quadrupole (TQ) ICP-MS at Michigan State University, employing similar techniques. For the latter, Ca, I, and Mg were each measured in both single-quadrupole and triplequadrupole modes. Freshly made iodine calibration solutions (iodide solution, I.V. Labs, Inc., with 50 ppm [Ca]), calcium calibration solutions standards and blank solutions containing 0.5% TMAH and 0.5% nitric acid were analysed routinely to monitor contributions from processing blanks and instrument memory, which were all matrix-matched with all the samples. ICP-MS standards (Cs, In, Sc) were added to each sample and calibration solution as internal standards and used to normalize the target analytes. A calibration line was produced every 5 to 8 blocks to correct instrumental drift, and data were corrected using the slope of the drift monitors over time. Reference material in-house standard (Porites coral; aragonite) and international standard JCp-1 (Porites coral; aragonite) were measured after every 5 to 8 samples.

In-house coral standard (*Porites* coral; aragonite) showed consistency within the run, and the I/Ca value yielded 3.58 \pm 0.36 $\mu mol/mol$ (1 $\sigma,$ n = 24). To compare data between labs, the I/Ca value of JCp-1 for all batches measured at WHOI is 3.91 \pm 0.36 $\mu mol/mol$ (1 $\sigma,$ n = 34), and at Michigan State University is 4.09 \pm 0.34 $\mu mol/mol$ (1 $\sigma,$ n = 7). Both results are within the uncertainty of published I/Ca values, where 3.70 \pm 0.27 $\mu mol/mol$ (1 $\sigma,$ n = 2280) in Lu et al. (2020c) and 4.12 \pm 0.26 $\mu mol/mol$ (1 $\sigma,$ n = 41) in Zhou et al. (2022). These standard data are shown in Supplementary Table 3.

For I/Ca data generated using the iCAP RQ ICP-MS, paired Mg/Ca data were separately measured on a Thermo Scientific Element2 ICP-MS at the University of Bristol. An aliquot of the dissolved sample (separate powder from I/Ca data) was analysed using well-characterized, matrix-matched, synthetic standard solutions to yield Mg/Ca ratios. Both NIST RM 8301-coral (simulated coral solution) and JCp-1 (uncleaned) carbonate reference materials were measured repeatedly and yielded a long-term analytical precision of $< \pm 2\%$ (1 σ).

3 Results

For scleractinian corals at all sites (n = 49), I/Ca varied from 4.81 to 13.64 μ mol/mol across seawater oxygen contents of 12 to 281 μ mol/kg (Figure 3; Supplementary Table 1). A key observation is that the I/Ca data can be separated into two groups at seawater O_2 concentration above and below 160 μ mol/kg. Samples with O_2 concentration < 160 μ mol/kg exhibit a mean I/Ca of 7.53 \pm 1.02 (RSD = 14%, n = 19), whereas the samples from O_2 concentration > 160 exhibit a mean I/Ca of 9.30 \pm 1.75 (RSD = 19%; n = 30). Though there is a slight overlap in the I/Ca of the two groups, they are nonetheless statistically significantly different (unequal variances t-test, t(46.78) = -4.47, p = 5.02e-05).

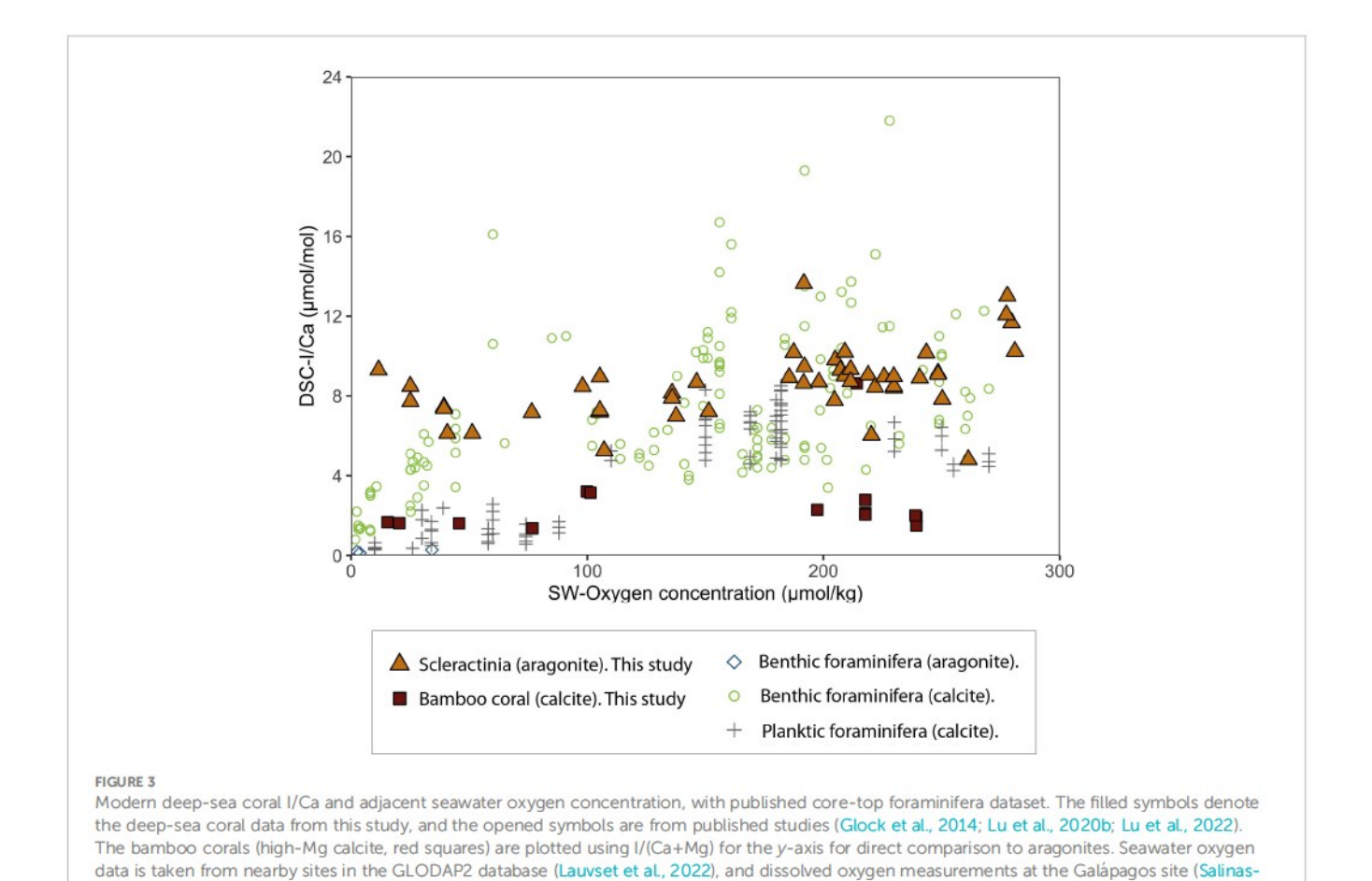
Bamboo corals are composed of high-Mg calcite; therefore, to compare results with scleractinian (aragonite) I/Ca data, we discuss the results in these samples regarding I/(Ca+Mg). The I/(Ca+Mg) of bamboo corals are in the range of 1.91 to 2.84 μ mol/mol within oxygen content of 20 to 240 μ mol/kg from Eastern North Pacific (n = 4) and Tropical North Atlantic (n = 9) (Figure 3; Supplementary Table 1). There is one exception for an outlier with an I/(Ca+Mg) value of 8.63 μ mol/mol in O2 concentration = 215 μ mol/kg. This outlier value is not included in further discussion. The bamboo coral I/(Ca+Mg) varied from 1.57 to 2.22 μ mol/mol. There are no significant differences across the oxygen concentrations range but a slight increase of I/(Ca+Mg) at O2 concentration >160 μ mol/kg (Supplementary Figure 3).

4 Discussion

I/Ca in marine carbonates, such as foraminifera, has shown the potential to record redox changes (Lu et al., 2020c). To explore this potential and iodine systematics in DSCs, we: (1) discuss the I/Ca ratios in different carbonate morphologies- aragonite and calcite, from two coral taxa; (2) discuss iodate incorporation mechanisms using seawater iodate concentration data and our coral I/Ca measurements; and (3) evaluate the potential of applying DSC I/Ca as a seawater oxygenation proxy.

4.1 Iodine concentration in aragonite versus calcite

Incorporating iodine species in calcium carbonate strongly depends on the mineral structure. Previous studies determined



the site location of iodine within carbonates. In contrast to most of the major/trace cations that exchange with Ca²⁺ in the carbonate structure, negatively charged iodine (as an iodate ion) has been confirmed to substitute for the carbonate ion in calcium carbonate (Podder et al., 2017). Results from computational simulations show that the iodate substitution into calcite involves a lower energy penalty than substitution into aragonite, meaning that iodate is preferentially partitioned into calcite over aragonite (Feng and Redfern, 2018). While incorporating iodate ion, the calcite lattice of the iodine-bearing structure remains the same (rhombohedral), but for iodine-bearing aragonite, the original orthorhombic cell reduces in symmetry to monoclinic. This leads to a large partitioning difference between calcite to aragonite.

de-León et al., 2020).

Surprisingly, our results show that the iodine concentration is higher in aragonitic scleractinian corals (mean I/Ca = 8.5 μmol/mol) compared to calcitic bamboo corals (mean I/Ca = 2.4 μmol/mol); Figure 3). This contradicts the results from computational simulations that predict a higher iodine relative abundance in calcite than in aragonite (Feng and Redfern, 2018). We emphasize that this comparison is done between I/Ca in scleractinian corals and I/(Ca+Mg) in bamboo corals, but since the iodate is substituting for the carbonate ion, the effect of higher Mg content in bamboo corals is minimal (Supplementary Figure 2). Additionally, the computational simulations were based on a concentrated iodate system with I/Ca ≈40 mmol/mol, almost 5,000 times higher than mean scleractinian

DSC I/Ca. Despite these substantial concentration differences, the results of iodate incorporation from our DSCs do not align with the enthalpic penalties and local distortion effects predicted by theoretical simulations. Previous studies noted inconsistencies between thermodynamic calculations and synthesis experiments in iodinebearing carbonate systems. For example, if thermodynamics are the only influence of iodate incorporation, increased temperature is expected to favor iodate incorporation due to the entropic advantage. However, the synthetic calcite experiment showed lower partition coefficients for iodate at higher temperatures (Zhou et al., 2014). In addition, the energetic penalty for iodate incorporation is less significant in vaterite than in calcite (Feng and Redfern, 2018), but synthesis experiments suggest that iodine is preferentially incorporated into calcite over vaterite (Podder et al., 2017). Moreover, simulation studies in calcite suggest a mechanism of surface segregation. From an entropy point of view, iodate could be more prone to substitute for CO32- in aragonite than calcite, as aragonite is more soluble than calcite (Mucci, 1983). These discrepancies, however, are largely unexplained and potential mechanisms remain a subject of speculation. These mechanisms include temperature-dependence of iodine speciation in aqueous solutions (Burns et al., 1990), and/or kinetic effects associated with carbonate dissolution and reprecipitation reactions.

Biological or 'vital' effects are another plausible control on iodine partitioning in DSCs. During coral calcification,

scleractinian coral increases the Ca concentration and pH of their calcifying fluid through the activity of the Ca/proton-pumps (Cohen and McConnaughey, 2003). This leads to a higher carbonate saturation, which favors aragonite precipitation. By contrast, bamboo corals experience a more complex anion exchange (bicarbonate), which includes a combination of Ca/ proton pumping and bicarbonate active transport, the latter of which has been proposed for sulfate incorporation (Flöter et al., 2022). Bicarbonate active transport delivers bicarbonate to the calcifying fluid to keep the calcite saturation at a high level and increases carbonate ion concentration by shifting the calcifying fluid pH. This process leads to a decrease in the calcifying fluid sulphur:carbonate ratio and thus a decrease in bamboo coral skeletal S:Ca ratio. This is also supported by a calcifying fluid study and boron isotope measurements that suggested bamboo corals undergo a minimal modification of their internal pH compared to scleractinian corals (Farmer et al., 2015). As sulfate also replaces the carbonate ion in the carbonate lattice, an analogous mechanism may be involved in iodate incorporation. The additional bicarbonate active transport in bamboo corals may be responsible for their lower I/Ca values compared to scleractinian corals. We thus argue that the biological control on iodate partitioning between different DSC families represents a more robust control than mineralogical differences.

Further studies are required to better understand iodine incorporation, including the divergent results from the thermodynamic calculation and experimental measurements, the factors controlling over iodine incorporation (e.g., pH, temperature), the growth rate effects of biogenic carbonate during calcification, and DSC culture experiments of iodine uptake. This also highlights the need for biogenic carbonate studies to consider a group-specific classification, such as family, genus, or species when developing proxy applications (e.g., Kershaw et al., 2023).

4.2 Scleractinian coral I/Ca and its incorporation

With the large difference in iodine concentration in DSCs due to their carbonate structures reported here, we first focus on scleractinian coral (aragonite) and investigate the potential controlling factors of I/Ca. Scleractinian coral I/Ca increases with seawater iodate concentration, except for samples from high latitudes (Figure 4B). A similar relationship has been reported in synthesis experiments for calcite, with a significant linear correlation between calcite I/Ca and ambient water iodate concentration (Lu et al., 2010; Zhou et al., 2014). Aragonitic coral I/Ca is overall higher than synthetic calcite I/Ca for a given water/ seawater iodate concentration (Figure 4B). With the exception of high latitude samples (North Atlantic and Southern Ocean), the slope of the linear regression line for the scleractinian corals is strikingly similar to that of the synthetic calcite (Figure 4B; Lu et al., 2010). This relationship suggests similar modes of incorporation of iodate into coral aragonite and synthetic calcite structures. Still, a few uncertainties may raise concerns about the findings. The calcite synthesis experiments were conducted in deionized water rather

than seawater, which may affect the incorporation of iodate. Also, this process was found to be temperature dependent, with greater incorporation at low temperatures and less at higher temperatures (Zhou et al., 2014). Nevertheless, the consistency between iodate incorporation into coral aragonite and synthetic calcite suggests that iodine in marine carbonate is incorporated mainly from surrounding seawater and in turn that the iodate concentration of ambient seawater could be a controlling factor for coral I/Ca.

In contrast, corals from high latitudes, specifically the North Atlantic and Southern Oceans, exhibit I/Ca ratios that deviate from values expected based on their nearby seawater iodate concentrations (450 to 500 nM; Figure 5). To further investigate this effect, we explore the secondary environmental controls on these samples. The I/Ca values do not correlate with seawater pH, [CO₃²⁻], dissolved phosphate concentrations, or dissolved nitrate concentrations at all sites (Supplementary Figure 1). However, on a regional scale, corals from the North Atlantic show that I/Ca and temperature have a negative correlation (Figure 5C). Also, I/Ca is negatively correlated with salinity (Figure 5D) due to the fact that seawater temperature and salinity are highly correlated at these sites. A similar negative correlation between I/Ca and temperature has also been reported in synthetic calcite experiments (Zhou et al., 2014) and core-top benthic foraminifera from the Little Bahama Bank region where oxygen concentrations are high (150 to 200 µmol/kg) (Lu et al., 2022). We speculate that, similar to benthic foraminifera, corals may naturally incorporate more iodate into their carbonate structure at lower temperatures. Another possible influencing factor is seasonal seawater iodate changes at high latitudes. Seawater iodate concentration at coastal Antarctic sites varies from 250 to 400 nM, with an interannual variability of around 160 nM (three observation years at 15 m depth) related to iodate reduction by biological productivity (Chance et al., 2010). Due to the limited longer-term seawater data, it is difficult to explore further the impact of temperature and seasonal iodate variation on coral I/Ca. Thus, further investigation of iodine incorporation into DSCs from high-latitude regions is needed.

The concentration of seawater iodate varies with oxygen content, and coral I/Ca ratios reflect these iodate concentrations; hence, this allows coral I/Ca to be used as a proxy for seawater oxygen content. Our results show that the coral I/Ca-O2 relationship undergoes an apparent "step change" at O2 concentration ≈ 160 µmol/kg, whereafter coral I/Ca remains elevated at high oxygen levels (Figure 4C). This significant step change is also present in both benthic and planktic foraminifera (Figure 3; Glock et al., 2014; Lu et al., 2020b; Lu et al., 2022), where a low O2 threshold for planktics occurs at around 100 µmol/kg (I/Ca < 2.5 µmol/mol), and for benthics at about 50 µmol/kg (I/Ca < 3 μmol/mol). Although the semi-quantitative I/Ca-O₂ relationships remain empirical, the oxygen thresholds in DSC I/Ca could correspond to their metabolic limits. Laboratory studies of Lophelia pertusa (scleractinian) have shown it maintains respiratory independence at high oxygen concentrations, but that respiration rate declines rapidly below a critical oxygen level of ~140 µmol/kg (Dodds et al., 2007). These results also agree with fieldbased population distributions in the North Atlantic, which indicate that DSCs are absent at the local oxygen minimum of around 150

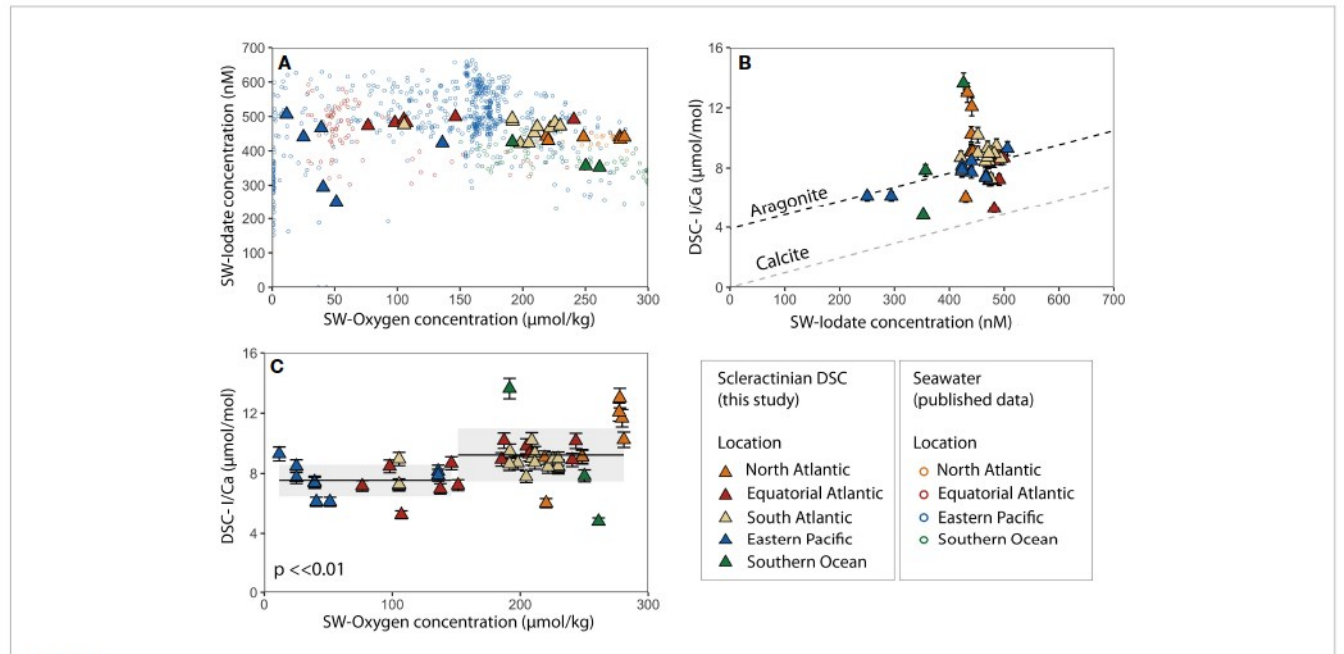
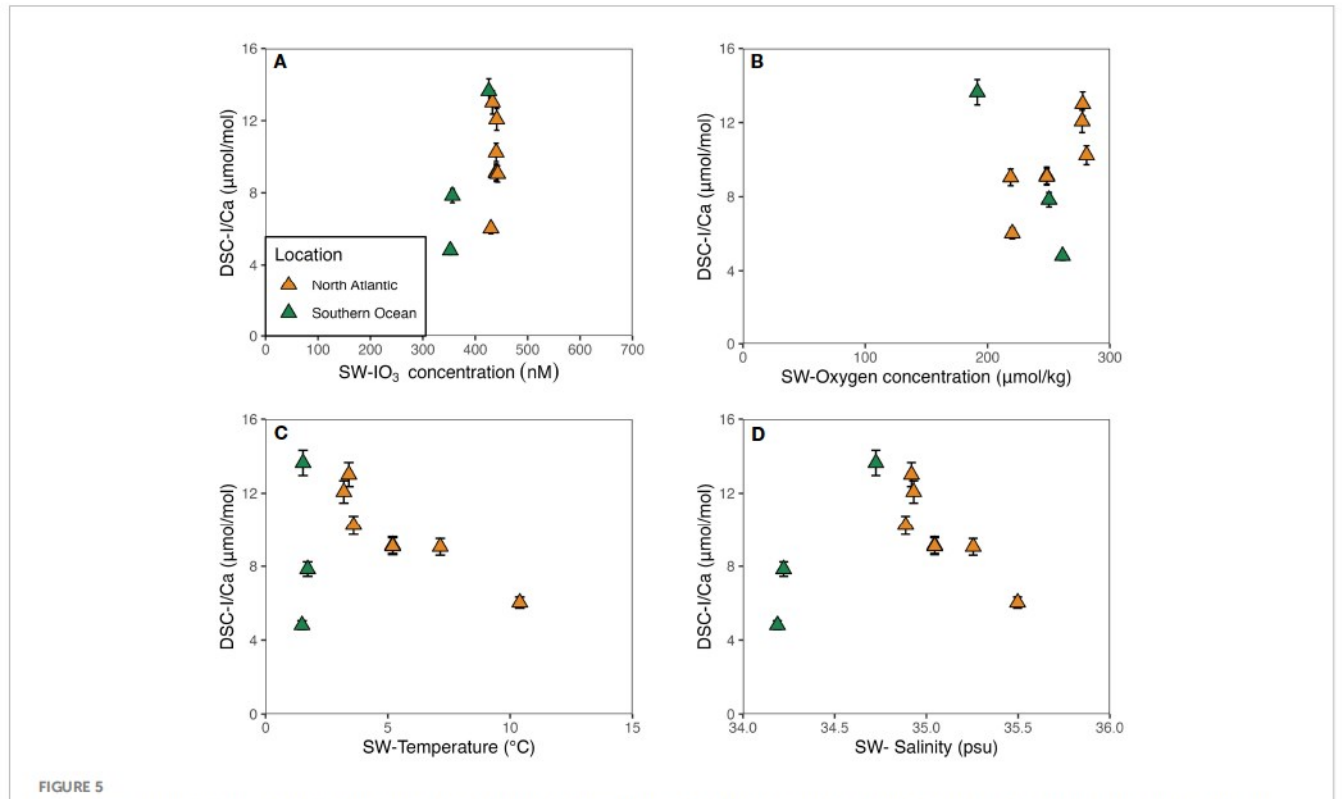


FIGURE 4
Cross-plots for scleractinian deep-sea coral (DSC) I/Ca and ambient seawater oxygen concentration. (A) Dissolved oxygen concentration versus dissolved iodate concentration in seawater. Proximal seawater iodate/iodide data were taken from published sources (Wong and Brewer, 1977; Elderfield and Truesdale, 1980; Bluhm et al., 2011; Cutter et al., 2018; Rapp et al., 2020). DSCs are in filled triangles and seawater data are in circles. The colours represent locations: North Atlantic (orange), Equatorial Atlantic (red), Southwest Atlantic (beige), Eastern Pacific (blue) and Southern Ocean (green). (B) Ambient seawater iodate concentration versus coral I/Ca. The black dashed line is a linear regression line of scleractinian DSC I/Ca (aragonite) without samples from the North Atlantic and Southern Ocean (y = 0.00937x + 3.90). The grey dashed line is the iodine incorporation results from calcite synthesis (y = 0.00974x; Lu et al., 2010). (C) Dissolved oxygen concentration versus I/Ca in deep-sea coral. The grey areas represent 1 SD. Error bar I/Ca in coral: $1 \sigma = 5\%$.



Deep-sea scleractinian coral (DSC) I/Ca values from high-latitude regions (North Atlantic and Southern Ocean) and ambient seawater parameters: (A) iodate concentration, (B) oxygen, (C) temperature, and (D) salinity. Paired seawater data are published iodate data (Elderfield and Truesdale, 1980; Bluhm et al., 2011), and the GLODAP 2 bottle database (Lauvset et al., 2022). Seawater temperature is positively correlated with salinity in the North Atlantic ($R^2 = 0.97$). The symbols used are identical to those in Figure 4. Error bar I/Ca in coral: 1 $\sigma = 5\%$.

 μ mol/kg (Thiagarajan et al., 2013). Further paleohabitat studies in the Southern Ocean also suggest that corals were less prevalent in the deep Polar Front (~1200 m depth) during the Antarctic Cold Reversal (14.7-13 ka), when seawater oxygen levels fell below this threshold. (Stewart et al., 2021). Together, these studies suggest DSCs have a change in biological function around an O₂ threshold at ~160 μ mol/kg, which could correspond to a potential change in iodate incorporation.

We next compare the I/Ca in aragonitic foraminifera versus aragonitic corals. The only I/Ca dataset from modern/recent aragonitic benthic foraminifera is Hoeglundina elegans from OMZs off the Peru margin, which suggests no significant correlation between I/Ca and bottom water oxygen concentration (Glock et al., 2014). These authors concluded that this might be due to the dissolution and recrystallisation of metastable aragonite that can happen at the early stage of diagenesis, thus altering I/Ca ratios. However, their study only focused on extremely low dissolved oxygen content (< 10 µmol/kg), meaning iodate reduction had occurred and making iodide the prevalent iodine species in this setting. The I/Ca data only varies in a relatively small range (~0.1 to 0.3 µmol/mol), which makes it difficult to detect significant variations. Our results for DSCs argue against this finding and suggest that I/Ca in aragonite could reflect seawater oxygen content. The low aragonitic H. elegans I/Ca versus higher I/Ca in scleractinian corals at locations with O2 concentrations < ~50 µmol/kgare possibly due to the difference in seawater iodate concentrations and/or regional water mass mixing processes related to their locations (i.e., H. elegans were collected at OMZs off Peruvian margin; scleractinian corals were collected at OMZ closer to the equator), or the difference between foraminifera and DSC calcification processes.

Lastly, we find no significant oxygen threshold in our bamboo coral I/Ca results, but a hint of a slight increase of I/Ca values at $\rm O_2$ concentration < ~160 umol/kg (Supplementary Figure 3). This could be explained by reduced vital effects in bamboo corals (Section 4.1) and/or sampling biases given the limited available data. Additional calibration studies of bamboo corals are required before they can be used to study paleo-oxygenation. Due to these limitations, we focus on the potential use of scleractinian corals for future proxy applications.

4.3 Implications for the DSC I/Ca paleo-oxygenation proxy

Here, we propose that iodate incorporation in deep-sea corals is linked to seawater oxygen content. Scleractinian corals exhibit a "step-change" in I/Ca at an O_2 concentration $\approx 160 \mu mol/kg$, which may be further utilized as an indicator to reconstruct marine oxygen content similarly to I/Ca measurements in foraminifera (e.g., Lu et al., 2020c).

Decreasing marine dissolved oxygen content as a result of global warming is predicted to accelerate in the near future (Oschlies et al., 2018). Due to the probable threat to marine ecosystems, understanding the linkages between the carbon and oxygen cycles is vital. Scleractinian DSCs offer a promising, well-dated archive of past oceanic environments, and by applying an I/Ca-oxygenation proxy, the reconstructed oxygenation records could shed new light

on key paleoclimate events. For example, during the last ice age, the deep Pacific is thought to have stored more respired carbon when oxygen-depleted deep waters were expanded in the eastern tropical Pacific (Hoogakker et al., 2018). However, redox proxies commonly used to tackle this issue, such as authigenic uranium, benthic foraminifera carbon isotope gradients and biomarker preservation, sometimes yield different oxygen-level reconstructions due to the limitations of each proxy (Jacobel et al., 2020). The DSC I/Ca proxy has the advantage of recording variations in intermediate water masses, providing an independent proxy perspective on oxygen reconstructions. For example, glacial to modern seawater O2 concentration in the South Indian Ocean is suggested to have increased from ~100 to ~220 µmol/kg (Gottschalk et al., 2020). This range covers our coral I/Ca-O2 threshold and provides an alternative archive to study deep-ocean oxygenation, focusing on abrupt events during the last millennium owing to the absolute radiometric dating potential of DSCs.

One potential obstacle to utilizing the I/Ca proxy in scleractinian coral is the biological behavior under low oxygen conditions (e.g., Hughes et al., 2020). Recent studies have shown that DSCs are able to thrive under hypoxic environments (e.g., Hebbeln et al., 2020; Salinas-de-León et al., 2020), but the question remains whether DSCs would modify their calcification to adopt to extreme conditions. For example, Lophelia pertusa would exhibit high mortality to maintain respiratory competence under low O₂ concentration by utilizing polyp expansion to increase tissue surface area and facilitate a diffusive gas exchange (Dodds et al., 2007). However, whether these processes would affect iodate incorporation during coral skeleton formation is unknown. Culture studies are therefore required to further explore the I/Ca ratio in DSCs as an oxygenation proxy. Nevertheless, DSCs serve as a potential archive that will allow us to indicate marine oxygen concentration above or below a specific level in the past.

5 Conclusions

Our study provides insight into the incorporation mechanisms of iodine into deep-sea corals (DSCs) and its potential as a proxy for seawater oxygenation. Contrary to computational simulations suggesting that iodate preferentially partitions into calcite over aragonite, our findings show that scleractinian corals (aragonitic) generally exhibit higher I/Ca than bamboo corals (calcitic). This suggests that biological processes exert a stronger control over iodine incorporation into DSC skelektons than mineralogical differences. For scleractinian corals, the potential main controlling factor on coral I/Ca is the iodate concentration of ambient seawater, except for a few high-latitude samples that potentially exhibit a strong secondary temperature/salinity influence. The I/Ca of bamboo corals does not appear to be sensitive to ambient iodate—and, by extension, oxygen—concentrations, which may relate to biological influences on calcification.

Overall, our data suggest that scleractinian DSCs have the potential to track water mass dissolved O_2 content at a certain level, as evidenced by a significant I/Ca "step change" occurring at oxygen concentrations around 160 μ mol/kg. This relationship can provide an independent perspective on seawater O_2 concentration reconstructions that may help resolve discrepancies between

existing oxygenation proxies. Our study provides a first-order empirical understanding of the I/Ca systematics of natural corals and their relationship with the ambient seawater characteristics. This reveals the potential of DSC I/Ca to reconstruct past changes in oxygen levels of water masses and improve our understanding of Earth's biogeochemical history.

Data availability statement

The original contributions presented in the study are included in the article/Supplementary Material. Further inquiries can be directed to the corresponding author.

Author contributions

YS: Conceptualization, Data curation, Funding acquisition, Investigation, Writing – original draft. LR: Conceptualization, Funding acquisition, Resources, Supervision, Writing – original draft, Writing – review & editing. IP: Supervision, Writing – original draft, Writing – review & editing. JS: Supervision, Writing – original draft, Writing – review & editing. WL: Investigation, Methodology, Writing – review & editing. DH: Investigation, Resources, Writing – review & editing. JK: Resources, Writing – review & editing. TH: Conceptualization, Investigation, Resources, Writing – original draft, Writing – review & editing.

Funding

The author(s) declare financial support was received for the research, authorship, and/or publication of this article. Funding for this work was provided by a bursary from Antarctic Science Ltd. and a Government Scholarship Program for overseas study from the Ministry of Education, Taiwan awarded to Y-J.S, and NERC grants awarded to LR (NE/S001743/1; NE/R005117/1; NE/N003861/1; NE/X00127X/1). Cruise DY081 was funded by the European Research Council starting grant ICY-LAB (Grant Agreement 678371). TH acknowledges support from the Woods Hole Oceanographic Institution's President's Innovation Fund and The Breene M. Kerr Early Career Scientist Endowment Fund. DH thanks NSF CO award # 1829406.

Acknowledgments

We acknowledge the crew and researchers on board the research vessels that obtained the samples for this study. We thank the Charles Darwin Foundation, Galápagos National Park,

and INOCAR for Galápagos sampling. AL0508 was supported by The Dalio Explore Fund. We also acknowledge the Galápagos National Park directorate for permission to map and collect submarine rock and biological samples (PC-44-15) and the Charles Darwin Foundation for facilitating scientific collaboration in the Galápagos. Access to specimens from the Muséum National d'Histoire Naturelle (MNHN, Paris) was facilitated by Magalie Castelin (Cnidaria curator) and Jonathan Blettery (SYNTHESYS+, a grant awarded to James Kershaw). MNHN specimens were obtained during expedition MUSORSTOM 9, organised by the MNHN and the Institut de Recherche pour le Développement as part of the Tropical Deep-Sea Benthos program (previously MUSORSTOM). The authors are grateful to the cruise leader, Bertrand Richer de Forges, and to Helmut Zibrowius who identified the specimens. We acknowledge the support from Konrad Hughen providing international and in-house coral standards for iodine measurement. We thank Keyi Cheng, Maureen Auro, Jerzy S Blusztajn, Christopher D Coath, Jamie Lewis, Carolyn Taylor, Maria Luiza De Carvalho Ferreira, Yingchu Shen and Maoyu Wang for their help with laboratory work. We thank Jui-Yen Lin and Kuan-Yu Lin for the discussions on iodine speciation thermodynamics. We thank Zunli Lu and George W Luther as well as the Editor Alex J Poulton for their constructive comments that greatly improved the manuscript.

Conflict of interest

The authors declare that the research was conducted in the absence of any commercial or financial relationships that could be construed as a potential conflict of interest.

The reviewer ZL declared a past co-authorship with the author WL to the handling Editor.

Publisher's note

All claims expressed in this article are solely those of the authors and do not necessarily represent those of their affiliated organizations, or those of the publisher, the editors and the reviewers. Any product that may be evaluated in this article, or claim that may be made by its manufacturer, is not guaranteed or endorsed by the publisher.

Supplementary material

The Supplementary Material for this article can be found online at: https://www.frontiersin.org/articles/10.3389/fmars.2023.1264380/full#supplementary-material

References

Barker, S., Greaves, M., and Elderfield, H. (2003). A study of cleaning procedures used for foraminiferal Mg/Ca paleothermometry: MG/CA PALEOTHERMOMETRY. Geochem. Geophys. Geosyst. 4, n/a–n/a. doi: 10.1029/2003GC000559

Bluhm, K., Croot, P. L., Huhn, O., Rohardt, G., and Lochte, K. (2011). Distribution of iodide and iodate in the Atlantic sector of the southern ocean during austral summer. Deep Sea Res. Part II: Topical Stud. Oceanography 58, 2733–2748. doi: 10.1016/j.idsr2.2011.02.002

Broecker, W. S., and Peng, T. H. (1982). *Tracers in the Sea* (Palisades, New York: Lamont-Doherty Geological Observatory, Columbia University).

Burns, W. G., Matsuda, M., and Sims, H. E. (1990). Temperature dependence of the equilibrium constant for iodine hydrolysis at temperatures between 25 and 120 °C. *J. Chem. Soc. Faraday Trans.* 86, 1443–1447. doi: 10.1039/FT9908601443

Campos, M. L. A. M., Farrenkopf, A. M., Jickells, T. D., and Luther, G. W. (1996). A comparison of dissolved iodine cycling at the Bermuda Atlantic Time-series Station and Hawaii Ocean Time-series Station. *Deep Sea Res. Part II: Topical Stud. Oceanography* 43, 455–466. doi: 10.1016/0967-0645(95)00100-X

Carpenter, L. J., Chance, R. J., Sherwen, T., Adams, T. J., Ball, S. M., Evans, M. J., et al. (2021). Marine iodine emissions in a changing world. *Proc. R. Soc A.* 477, 20200824. doi: 10.1098/rspa.2020.0824

Carpenter, L. J., MacDonald, S. M., Shaw, M. D., Kumar, R., Saunders, R. W., Parthipan, R., et al. (2013). Atmospheric iodine levels influenced by sea surface emissions of inorganic iodine. *Nat. Geosci* 6, 108–111. doi: 10.1038/ngeo1687

Chance, R., Baker, A. R., Carpenter, L., and Jickells, T. D. (2014). The distribution of iodide at the sea surface. *Environ. Sci.: Processes Impacts* 16, 1841–1859. doi: 10.1039/C4EM00139G

Chance, R., Weston, K., Baker, A. R., Hughes, C., Malin, G., Carpenter, L., et al. (2010). Seasonal and interannual variation of dissolved iodine speciation at a coastal Antarctic site. *Mar. Chem.* 118, 171–181. doi: 10.1016/j.marchem.2009.11.009

Chen, T., Robinson, L. F., Burke, A., Southon, J., Spooner, P., Morris, P. J., et al. (2015). Synchronous centennial abrupt events in the ocean and atmosphere during the last deglaciation. *Science* 349, 1537–1541. doi: 10.1126/science.aac6159

Chen, T., Robinson, L. F., Li, T., Burke, A., Zhang, X., Stewart, J. A., et al. (2023). Radiocarbon evidence for the stability of polar ocean overturning during the Holocene. *Nat. Geosci.* 16, 631–636. doi: 10.1038/s41561-023-01214-2

Cheng, H., Adkins, J., Edwards, R. L., and Boyle, E. A. (2000). U-Th dating of deepsea corals. Geochimica Cosmochimica Acta 64, 2401–2416. doi: 10.1016/S0016-7037 (99)00422-6

Cohen, A. L., and McConnaughey, T. A. (2003). Geochemical perspectives on coral mineralization. *Rev. Mineralogy Geochemistry* 54, 151–187. doi: 10.2113/0540151

Cook, M. K., Dial, A. R., and Hendy, I. L. (2022). Iodine stability as a function of pH and its implications for simultaneous multi-element ICP-MS analysis of marine carbonates for paleoenvironmental reconstructions. *Mar. Chem.* 245, 104148. doi: 10.1016/j.marchem.2022.104148

Cutter, G. A., Moffett, J. W., Nielsdóttir, M. C., and Sanial, V. (2018). Multiple oxidation state trace elements in suboxic waters off Peru: *In situ* redox processes and advective/diffusive horizontal transport. *Mar. Chem.* 201, 77–89. doi: 10.1016/j.marchem.2018.01.003

Dickson, A. G., and Millero, F. J. (1987). A comparison of the equilibrium constants for the dissociation of carbonic acid in seawater media. *Deep Sea Res. Part A. Oceanographic Res. Papers* 34, 1733–1743. doi: 10.1016/0198-0149(87)90021-5

Dodds, L. A., Roberts, J. M., Taylor, A. C., and Marubini, F. (2007). Metabolic tolerance of the cold-water coral Lophelia pertusa (Scleractinia) to temperature and dissolved oxygen change. J. Exp. Mar. Biol. Ecol. 349, 205–214. doi: 10.1016/j.jembe.2007.05.013

Elderfield, H., and Truesdale, V. W. (1980). On the biophilic nature of iodine in seawater. Earth Planetary Sci. Lett. 50, 105–114. doi: 10.1016/0012-821X(80)90122-3

Evans, N., Boles, E., Kwiecinski, J. V., Mullen, S., Wolf, M., Devol, A. H., et al. (2020). The role of water masses in shaping the distribution of redox active compounds in the Eastern Tropical North Pacific oxygen deficient zone and influencing low oxygen concentrations in the eastern Pacific Ocean. *Limnol Oceanogr* 65, 1688–1705. doi: 10.1002/lno.11412

Farmer, J. R., Hönisch, B., Robinson, L. F., and Hill, T. M. (2015). Effects of seawater-pH and biomineralization on the boron isotopic composition of deep-sea bamboo corals. *Geochimica Cosmochimica Acta* 155, 86–106. doi: 10.1016/j.gca.2015.01.018

Farrenkopf, A. M., Dollhopf, M. E., Chadhain, S. N., Luther, G. W., and Nealson, K. H. (1997). Reduction of iodate in seawater during Arabian Sea shipboard incubations and in laboratory cultures of the marine bacterium Shewanella putrefaciens strain MR-4. Mar. Chem. 57, 347–354. doi: 10.1016/S0304-4203(97)00039-X

Farrenkopf, A. M., and Luther, G. W. (2002). Iodine chemistry reflects productivity and denitrification in the Arabian Sea: evidence for flux of dissolved species from sediments of western India into the OMZ. Deep Sea Res. Part II: Topical Stud. Oceanography 49, 2303–2318. doi: 10.1016/S0967-0645(02)00038-3

Feng, X., and Redfern, S. A. T. (2018). Iodate in calcite, aragonite and vaterite CaCO3: Insights from first-principles calculations and implications for the I/Ca geochemical proxy. Geochimica Cosmochimica Acta 236, 351–360. doi: 10.1016/j.gca.2018.02.017 Flöter, S., Fietzke, J., Gutjahr, M., Nehrke, G., and Eisenhauer, A. (2022). Incorporation of Na and S in bamboo coral skeletons. *Chem. Geology* 597, 120795. doi: 10.1016/j.chemgeo.2022.120795

Frenkel, M. M., LaVigne, M., Miller, H. R., Hill, T. M., McNichol, A., and Gaylord, M. L. (2017). Quantifying bamboo coral growth rate nonlinearity with the radiocarbon bomb spike: A new model for paleoceanographic chronology development. *Deep Sea Res. Part I: Oceanographic Res. Papers* 125, 26–39. doi: 10.1016/j.dsr.2017.04.006

Gagnon, A. C., Adkins, J. F., Fernandez, D. P., and Robinson, L. F. (2007). Sr/Ca and Mg/Ca vital effects correlated with skeletal architecture in a scleractinian deep-sea coral and the role of Rayleigh fractionation. *Earth Planetary Sci. Lett.* 261, 280–295. doi: 10.1016/j.epsl.2007.07.013

García-Ibáñez, M. I., Pérez, F. F., Lherminier, P., Zunino, P., Mercier, H., and Tréguer, P. (2018). Water mass distributions and transports for the 2014 GEOVIDE cruise in the North Atlantic. *Biogeosciences* 15, 2075–2090. doi: 10.5194/bg-15-2075-2018

Geyman, B. M., Ptacek, J. L., LaVigne, M., and Horner, T. J. (2019). Barium in deepsea bamboo corals: Phase associations, barium stable isotopes, & prospects for paleoceanography. *Earth Planetary Sci. Lett.* 525, 115751. doi: 10.1016/ j.epsl.2019.115751

Glock, N., Liebetrau, V., and Eisenhauer, A. (2014). I/Ca ratios in benthic foraminifera from the Peruvian oxygen minimum zone: analytical methodology and evaluation as a proxy for redox conditions. *Biogeosciences* 11, 7077–7095. doi: 10.5194/bg-11-7077-2014

Gottschalk, J., Michel, E., Thöle, L. M., Studer, A. S., Hasenfratz, A. P., Schmid, N., et al. (2020). Glacial heterogeneity in Southern Ocean carbon storage abated by fast South Indian deglacial carbon release. *Nat. Commun.* 11, 6192. doi: 10.1038/s41467-020-20034-1

Hardisty, D. S., Horner, T. J., Evans, N., Moriyasu, R., Babbin, A. R., Wankel, S. D., et al. (2021). Limited iodate reduction in shipboard seawater incubations from the Eastern Tropical North Pacific oxygen deficient zone. *Earth Planetary Sci. Lett.* 554, 116676. doi: 10.1016/j.epsl.2020.116676

Hartin, C. A., Fine, R. A., Sloyan, B. M., Talley, L. D., Chereskin, T. K., and Happell, J. (2011). Formation rates of Subantarctic mode water and Antarctic intermediate water within the South Pacific. *Deep Sea Res. Part I: Oceanographic Res. Papers* 58, 524–534. doi: 10.1016/j.dsr.2011.02.010

Hashim, M. S., Burke, J. E., Hardisty, D. S., and Kaczmarek, S. E. (2022). Iodine incorporation into dolomite: Experimental constraints and implications for the iodine redox proxy and Proterozoic Ocean. *Geochimica Cosmochimica Acta* 338, 365–381. doi: 10.1016/j.gca.2022.10.027

Haynes, W. M. (Ed.). (2014). CRC Handbook of Chemistry and Physics (Boca Raton, FL, USA: CRC Press). doi: 10.1201/b17118

Hebbeln, D., Wienberg, C., Dullo, W.-C., Freiwald, A., Mienis, F., Orejas, C., et al. (2020). Cold-water coral reefs thriving under hypoxia. *Coral Reefs* 39, 853–859. doi: 10.1007/s00338-020-01934-6

Hoogakker, B. A. A., Lu, Z., Umling, N., Jones, L., Zhou, X., Rickaby, R. E. M., et al. (2018). Glacial expansion of oxygen-depleted seawater in the eastern tropical Pacific. *Nature* 562, 410–413. doi: 10.1038/s41586-018-0589-x

Hughes, D. J., Alderdice, R., Cooney, C., Kühl, M., Pernice, M., Voolstra, C. R., et al. (2020). Coral reef survival under accelerating ocean deoxygenation. *Nat. Clim. Change* 10, 296–307. doi: 10.1038/s41558-020-0737-9

Jacobel, A. W., Anderson, R. F., Jaccard, S. L., McManus, J. F., Pavia, F. J., and Winckler, G. (2020). Deep Pacific storage of respired carbon during the last ice age: Perspectives from bottom water oxygen reconstructions. *Quaternary Sci. Rev.* 230, 106065. doi: 10.1016/j.quascirev.2019.106065

Kerisit, S. N., Smith, F. N., Saslow, S. A., Hoover, M. E., Lawter, A. R., and Qafoku, N. P. (2018). Incorporation modes of iodate in calcite. *Environ. Sci. Technol.* 52, 5902–5910. doi: 10.1021/acs.est.8b00339

Kershaw, J., Stewart, J. A., Strawson, I., de Carvalho Ferreira, M. L., Robinson, L. F., Hendry, K. R., et al. (2023). Ba/Ca of stylasterid coral skeletons records dissolved seawater barium concentrations. *Chem. Geology* 622, 121355. doi: 10.1016/j.chemgeo.2023.121355

Lauvset, S. K., Lange, N., Tanhua, T., Bittig, H. C., Olsen, A., Kozyr, A., et al. (2022). GLODAPv2.2022: the latest version of the global interior ocean biogeochemical data product. *Earth Syst. Sci. Data* 14, 5543–5572. doi: 10.5194/essd-14-5543-2022

Liu, M., and Tanhua, T. (2021). Water masses in the Atlantic Ocean: characteristics and distributions. *Ocean Sci.* 17, 463–486. doi: 10.5194/os-17-463-2021

Lu, W., Dickson, A. J., Thomas, E., Rickaby, R. E. M., Chapman, P., and Lu, Z. (2020a). Refining the planktic foraminiferal I/Ca proxy: Results from the Southeast Atlantic Ocean. *Geochimica Cosmochimica Acta* 287, 318–327. doi: 10.1016/j.gca.2019.10.025

Lu, W., Rickaby, R. E. M., Hoogakker, B. A. A., Rathburn, A. E., Burkett, A. M., Dickson, A. J., et al. (2020b). I/Ca in epifaunal benthic foraminifera: A semi-quantitative proxy for bottom water oxygen in a multi-proxy compilation for glacial ocean deoxygenation. *Earth Planetary Sci. Lett.* 533, 116055. doi: 10.1016/j.epsl.2019.116055

- Lu, W., Wang, Y., Oppo, D. W., Nielsen, S. G., and Costa, K. M. (2022). Comparing paleo-oxygenation proxies (benthic foraminiferal surface porosity, I/Ca, authigenic uranium) on modern sediments and the glacial Arabian Sea. *Geochimica Cosmochimica Acta* 331, 69–85. doi: 10.1016/j.gca.2022.06.001
- Lu, Z., Jenkyns, H. C., and Rickaby, R. E. M. (2010). Iodine to calcium ratios in marine carbonate as a paleo-redox proxy during oceanic anoxic events. *Geology* 38, 1107–1110. doi: 10.1130/G31145.1
- Lu, Z., Lu, W., Rickaby, R. E. M., and Thomas, E. (2020c). Earth History of Oxygen and the iprOxy (Elements in Geochemical Tracers in Earth System Science). (Cambridge: Cambridge University Press). doi: 10.1017/9781108688604
- Lu, Z., Hoogakker, B. A. A., Hillenbrand, C.-D., Zhou, X., Thomas, E., Gutchess, K. G., et al. (2016). Oxygen depletion recorded in upper waters of the glacial Southern Ocean. *Nat. Commun.* 7, 11146. doi: 10.1038/ncomms11146
- Luther, G. W. (2023). Review on the physical chemistry of iodine transformations in the oceans. Front. Mar. Sci. 10. doi: 10.3389/fmars.2023.1085618
- Moriyasu, R., Bolster, K. M., Hardisty, D. S., Kadko, D. C., Stephens, M. P., and Moffett, J. W. (2023). Meridional survey of the central pacific reveals iodide accumulation in equatorial surface waters and benthic sources in the abyssal plain. Global Biogeochemical Cycles 37, e2021GB007300. doi: 10.1029/2021GB007300
- Moriyasu, R., Evans, N., Bolster, K. M., Hardisty, D. S., and Moffett, J. W. (2020). The distribution and redox speciation of iodine in the Eastern Tropical North Pacific Ocean. *Global Biogeochem. Cycles* 34. doi: 10.1029/2019GB006302
- Mucci, A. (1983). The solubility of calcite and aragonite in seawater at various salinities, temperatures, and one atmosphere total pressure. Am. J. Sci. 283, 780–799. doi: 10.2475/ajs.283.7.780
- Orejas, C., Wienberg, C., Titschack, J., Tamborrino, L., Freiwald, A., and Hebbeln, D. (2021). Madrepora oculata forms large frameworks in hypoxic waters off Angola (SE Atlantic). Sci. Rep. 11, 15170. doi: 10.1038/s41598-021-94579-6
- Oschlies, A., Brandt, P., Stramma, L., and Schmidtko, S. (2018). Drivers and mechanisms of ocean deoxygenation. *Nat. Geosci* 11, 467–473, doi: 10.1038/s41561-018-0152-2
- Pelletier, G. J., Lewis, E., and Wallace, D. (2007). CO2SYS. XLS: A calculator for the CO2 system in seawater for Microsoft Excel/VBA. (Olympia, WA/Upton, NY, USA: Washington State Department of Ecology/Brookhaven National Laboratory).
- Peters, B. D., Jenkins, W. J., Swift, J. H., German, C. R., Moffett, J. W., Cutter, G. A., et al. (2018). Water mass analysis of the 2013 US GEOTRACES eastern Pacific zonal transect (GP16). *Mar. Chem.* 201, 6–19. doi: 10.1016/j.marchem.2017.09.007
- Podder, J., Lin, J., Sun, W., Botis, S. M., Tse, J., Chen, N., et al. (2017). Iodate in calcite and vaterite: Insights from synchrotron X-ray absorption spectroscopy and first-principles calculations. *Geochimica Cosmochimica Acta* 198, 218–228. doi: 10.1016/j.gca.2016.11.032
- Rapp, I., Schlosser, C., Browning T. J., Wolf, F., Le Moigne, F. A. C., Gledhill, M., et al. (2020). El Niño-driven oxygenation impacts Peruvian shelf iron supply to the South Pacific Ocean. *Geophys. Res. Lett.* 47. doi: 10.1029/2019GL086631
- Roberts, J. M., Wheeler, A. J., and Freiwald, A. (2006). Reefs of the deep: The biology and geology of cold-water coral ecosystems. Science 312, 543-547. doi: 10.1126/science.1119861

- Robinson, L. F., Adkins, J. F., Frank, N., Gagnon, A. C., Prouty, N. G., Brendan Roark, E., et al. (2014). The geochemistry of deep-sea coral skeletons: A review of vital effects and applications for palaeoceanography. *Deep Sea Res. Part II: Topical Stud. Oceanography* 99, 184–198. doi: 10.1016/j.dsr2.2013.06.005
- Ross, T., Du Preez, C., and Ianson, D. (2020). Rapid deep ocean deoxygenation and acidification threaten life on Northeast Pacific seamounts. *Global Change Biol.* 26, 6424–6444. doi: 10.1111/gcb.15307
- Rue, E. L., Smith, G. J., Cutter, G. A., and Bruland, K. W. (1997). The response of trace element redox couples to suboxic conditions in the water column. *Deep Sea Res. Part I: Oceanographic Res. Papers* 44, 113–134. doi: 10.1016/S0967-0637(96)00088-X
- Salinas-de-León, P., Martí-Puig, P., Buglass, S., Arnés-Urgellés, C., Rastoin-Laplane, E., Creemers, M., et al. (2020). Characterization of deep-sea benthic invertebrate megafauna of the Galapagos Islands. Sci. Rep. 10, 13894. doi: 10.1038/s41598-020-70744-1
- Stewart, J. A., Li, T., Spooner, P. T., Burke, A., Chen, T., Roberts, J., et al. (2021). Productivity and dissolved oxygen controls on the Southern Ocean Deep-Sea Benthos during the antarctic cold reversal. *Paleoceanog Paleoclimatol* 36, e2021PA004288. doi: 10.1029/2021PA004288
- Stewart, J. A., Robinson, L. F., Day, R. D., Strawson, I., Burke, A., Rae, J. W. B., et al. (2020). Refining trace metal temperature proxies in cold-water scleractinian and stylasterid corals. *Earth Planetary Sci. Lett.* 545, 116412. doi: 10.1016/j.epsl.2020.116412
- Sumida, P. Y. G., Bernardino, A. F., and De Léo, F. C. (2020). *Brazilian Deep-Sea Biodiversity*. (Cham: Springer International Publishing). doi: 10.1007/978-3-030-53222-2
- Thiagarajan, N., Gerlach, D., Roberts, M. L., Burke, A., McNichol, A., Jenkins, W. J., et al. (2013). Movement of deep-sea coral populations on climatic timescales: CORAL POPULATIONS AND CLIMATE. *Paleoceanography* 28, 227–236. doi: 10.1002/palo.20023
- Truesdale, V. W., Bale, A. J., and Woodward, E. M. S. (2000). The meridional distribution of dissolved iodine in near-surface waters of the Atlantic Ocean. *Prog. Oceanography* 45, 387–400. doi: 10.1016/S0079-6611(00)00009-4
- Winkelbauer, H., Cordova-Rodriguez, K., Reyes-Macaya, D., Scott, J., Glock, N., Lu, Z., et al. (2021). Foraminifera iodine to calcium ratios: approach and cleaning. *Geochem Geophys Geosyst* 22. doi: 10.1029/2021GC009811
- Wong, G. T. F., and Brewer, P. G. (1977). The marine chemistry of iodine in anoxic basins. *Geochimica Cosmochimica Acta* 41, 151–159. doi: 10.1016/0016-7037(77) 90195-8
- Zhou, X., Hess, A. V., Bu, K., Sagawa, T., and Rosenthal, Y. (2022). Simultaneous determination of I/ca and other elemental ratios in foraminifera: comparing results from acidic and basic solutions. *Geochem Geophys Geosyst* 23. doi: 10.1029/2022GC010660
- Zhou, X., Thomas, E., Rickaby, R. E. M., Winguth, A. M. E., and Lu, Z. (2014). I/Ca evidence for upper ocean deoxygenation during the PETM. *Paleoceanography* 29, 964–975. doi: 10.1002/2014PA002702